Nanoscale

Accepted Manuscript

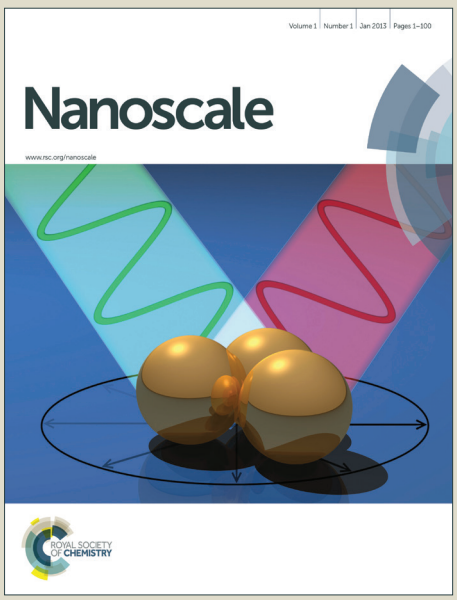

ROYAL SOCIETY OF CHEMISTRY

www.rsc.org/nanoscale

Nanoscale

RSCPublishing

ARTICLE

Large-Scale, Low-Cost Synthesis of Monodispersed Gold Nanorods by Using A Gemini Surfactant

Cite this: DOI: 10.1039/xoxxoooooox

Yong Xu,[§] Yang Zhao,[§] Lei Chen, Xuchun Wang, Jianxia Sun, Haihua Wu, Feng Bao, Jian Fan, Qiao Zhang*

Received ooth January 2012,
Accepted ooth January 2012

DOI: 10.1039/xoxxoooooox

www.rsc.org/

In this work, we demonstrate that monodispersed gold nanorods (AuNRs) can be obtained in a large-scale and cost-effective way. By using an industrial grade Gemini surfactant (P16-8-16), the cost of the synthesis of high-quality AuNRs can be significantly reduced by 90%. The synthesis can be scaled up to over 4 L. The aspect ratio of AuNRs can be well tuned from ~2.4 to ~6.3, resulting in a wide tunability of the SPR property. Systematic studies reveal that P16-8-16 could have dual functions: it can not only act as a capping ligand to stabilize AuNRs but also can pre-reduce Au^{3+} to Au^{+} by the unsaturated C=C bond. Furthermore, the shape of AuNRs can be tailored from straight nanorods to "dog-bones" by simply varying the concentration of surfactant. Mechanistic study shows that the shape change can be attributed to the presence of excess bromide ions because of the complex effect between bromide ions and gold ions. This work will not only help to achieve industrial production of AuNRs, but also promote the research in the practical applications of various nanomaterials.

Introduction

Nanomaterials have attracted increasing attention due to their promising applications in diverse fields.[1-3] With the development of nanotechnology over the past decades, researchers are able to synthesize nanomaterials with various shapes and controllable dimensions, including zero-dimensional (nanospheres and nanoshells),[4-6] one-dimensional (nanorods and nanowires),[7-10] two-dimensional (nanoplates, nanoprisms, nanosheets, nanodisks),[11, 12] and three-dimensional nanoparticles (nanoflowers),[13] in an elegant manner. However, the practical applications of such nanomaterials have been seriously limited by several challenges, especially the low-volume production and high cost. It is thus highly desirable to develop synthetic protocols that can produce high-quality nanomaterials in a large-scale and cost-effective way.

As one of the most widely studied nanostructures, gold nanorods (AuNRs) have drawn much attention because of their high anisotropy and promising applications in many fields, such as photothermal therapy,[14-16] diagnosis,[17, 18] biomedicine,[19, 20] sensing,[21-23] surface-enhanced Raman scattering (SERS),[24, 25] and so forth. Although impressive progress has been achieved in AuNRs synthesis, some challenges still remain, including lack of clear formation mechanism, low-volume production and high cost, which have seriously impeded its practical applications. Thanks to the pioneering work on the colloidal synthesis of AuNRs by Murphy, El-Sayed, Mulvaney, and Liz Marzán et al in the early 2000s,[26-28] we are able to synthesize high-quality AuNRs.[7, 29-31] However, to our best knowledge, all the reported protocols require high-purity reagents, because the quality of final product is very sensitive to the impurities. For example, it has been pointed out that some trace impurities, *e.g.*, iodide ions, can have noticeable effect on the quality of final product.[32-36] As a result, high-purity and expensive reagents are usually required to obtain high-quality AuNRs, resulting in the high cost of AuNRs synthesis. On the other hand, although the price of gold precursor is much higher than that of surfactant, the major cost is taken by surfactant, because its essential concentration is generally hundreds of times higher than that of gold precursor. For instance, the required concentration of hexadecyltrimethyl ammonium bromide (CTAB) is 100 mM in traditional silver-assisted seeded growth protocols, while the concentration of gold is only 0.25 mM.[37] As shown in Table 1, the estimated cost of CTAB is about 85 % of the total cost in the protocol developed by EI-Sayed and co-workers.[37] Although the recent work from Murray group and Xu group reported that the required concentration of surfactant can be significantly decreased by using binary surfactants containing CTAB (or CTAC hexadecyltrimethylammonium chloride,) and NaOL (sodium oleate), the estimated cost of surfactant is still over 50 % (Table 1).[10, 29,30] To meet the requirement of industrial application, one needs to develop a protocol that can synthesize AuNRs in a cost-effective way.

Recently, much effort has been paid to Gemini surfactant that contains two hydrophilic heads and two hydrophobic groups because of its superior property, such as lower critical micelle concentration (CMC) and higher surface activity, to corresponding conventional

surfactants.[38] It has been reported that Gemini surfactants can be used to prepare various gold nanostructures, including nanospheres,[39] nanoribbons,[40] and branched nanostructures.[41] Liz Marzán and co-workers demonstrated that monodispersed AuNRs can self-assemble into standing superlattices in the presence of (oligooxa) alkanediyl-α,ω-bis(dimethyldodecylammonium bromide) (12-EO$_x$-12), suggesting the important role of Gemini surfactant in the synthesis and self-assembly of anisotropic metal nanostructures.[42]

In this work, we report a robust method that can synthesize AuNRs with high morphological yield and tailored shapes in a large-scale and cost-effective way. An industrial grade Gemini surfactant, maleic acid diethyl bis(hexadecyl dimethyl ammonium bromide (P16-8-16, Figure 1a), that contains both alkyl quaternary ammonium ions and unsaturated carbon-carbon double bond, is used to replace the traditionally used CTAB or CTAC. In this protocol, the Gemini surfactant has dual functions: first, it is a good surfactant with low CMC (0.0235 mM), which is much lower than that of CTAB (0.1 mM);[37] second, the unsaturated C=C bond can pre-reduce Au^{3+} into Au^{+}, which might be a critical factor for making high-quality AuNRs.[7, 29, 30, 43] Compared to traditional silver-assisted seeded growth protocols using CTAB or CTAC, this method has several advantages. First, this protocol makes much cheaper AuNRs than that obtained from traditional protocols. Thanks to the unique features of the Gemini surfactant, one can use industrial grade surfactant instead of high-purity reagent. As shown in Table 1, the price of P16-8-16 is only about \$0.004/g, which is much lower than that of CTAB (\$0.29/g) or CTAC (\$0.6/g). Additionally, the required concentration of P16-8-16 is only 12 mM, which is also much lower than that of CTAB (100 mM in Ref. 37) or CTAC (37 mM in Ref. 29). As a result, the cost of surfactant is only about 0.7% of the total cost in this new protocol, making it promising for practical applications. Second, this method can be scaled up easily. In this work, we demonstrate that monodispersed AuNRs can be obtained from one large batch (as large as 4 L). Third, the shape of AuNRs can be tailored from nanorods to "dog-bones" by adjusting only the concentration of P16-8-16, which is more convenient than the reported methods that utilizes either by extending aging time [44] or by multi-step growth process that needs additional ascorbic acid.[45-47] Systematic studies reveal that the tailored shapes can be attributed to the kinetic effects of excess bromide ions.

Table 1.The estimated percentage of cost in the AuNRs synthesis using different protocols.

Protocols	Reagent	Concentration mM	Purity *wt.*%	Price US\$/g	Percentage of cost [a]
Ref.37	CTAB	100	99 %	1.8 [b]	85 %
	$HAuCl_4$	0.25	49 %	114.6 [b]	15 %
Ref.29	CTAC	37	98 %	0.6 [c]	44 %
	NaOL	10	97 %	1.1 [c]	20 %
	$HAuCl_4$	0.25	49 %	58.9 [d]	36 %
Ref.30	CTAB	37	98 %	0.29 [c]	30 %
	NaOL	10	50 %	1.1 [c]	26 %
	$HAuCl_4$	0.25	49 %	58.9 [d]	44 %
Present	P16-8-16	12	50 %	0.004 [e]	0.7 %
	$HAuCl_4$	0.25	49 %	114.6 [b]	99.3 %

Note: [a] the percentages are calculated by ignoring those very few parts (*e.g.*, AA, HCl); [b] the price is obtained from Sigma-Aldrich; [c] the price is obtained from TCI; [d] the price is obtained from Acros; [e] the price is obtained from Henan Daochun Co., LTD.

Experimental

Gold nanorods synthesis: Gold chloride trihydrate ($HAuCl_4 \cdot 3H_2O$), silver nitrate ($AgNO_3$, > 99 %), L-Ascorbic acid ($C_6H_8O_6$, > 99.7 %), sodium borohydride ($NaBH_4$, > 99 %) and potassium bromide (KBr, > 98.5 %) were obtained from Sigma-Aldrich. Hexadecyltrimethyl ammonium bromide ($C_{19}H_{42}BrN$, > 98 %) was purchased from TCI. P16-8-16 ($C_{44}H_{88}O_4N_2Br_2$, 50 wt% in water) was purchased from Henan Daochun Co., Ltd. A typical silver-assisted seeded growth was employed for synthesizing AuNRs. To prepare the seed solution, 10 mL of CTAB solution (0.2 M) was mixed with 10 mL $HAuCl_4$ (0.5 mM) in a 50 mL vial. 1.2 mL of ice-cold $NaBH_4$ (0.01 M) was diluted to 2 mL with ultra-pure water and was then injected to the Au(III) precursor solution under vigorous agitation (1100 rpm) for 1 min. The seed solution was aged at room temperature for at least 120 min before use. The growth solution with a total volume of 20 mL was prepared by adding $AgNO_3$ and $HAuCl_4$ into the P16-8-16 solution under moderate string. After about two hours, when the color changed from brownish to yellowish, HCl was added into the growth solution to adjust the pH value. After 15 min, ascorbic acid was added into the growth solution under rapid magnetic stirring for 30 seconds, followed by adding a certain amount of the prepared seed solution. After stirring for 2 min, the growth solution was kept undisturbed at room temperature overnight to allow the completion of reaction. For large-scale synthesis of AuNRs, 4,000 mL of P16-8-16 solution (0.12 mM) was added into a 5,000 mL flask with moderate stirring at room temperature, followed by the addition of 0.316 g $AgNO_3$ and 0.4 g $HAuCl_4$. When the color changed from brownish to yellowish, 2.7 mL of concentrated HCl (37 %) was added into the growth solution to adjust the pH value. 15 min later, 2 mL of ascorbic acid (0.64 M) was added into the growth solution under rapid stirring for 30 seconds, followed by adding 20 mL of the prepared seed solution. After stirring for 2 min, the growth solution was kept undisturbed at room temperature overnight to allow the completion of reaction.

Characterizations: Transmission electron microscopy (TEM) images were collected with a LaB6 TEM (TECNAI G2, FEI), operating at 200 KV. High resolution transmission electron microscope (HRTEM) images of the prepared AuNRs were obtained at 200 KV by using the model of Tecnai G2 F20 from FEI, USA. The UV-Vis spectra were obtained by using the LAMBDA 750 spectrograph in a range of 300-1200 nm from PERKINELMER, USA. Fourier transform infrared spectroscopy (FTIR) measurement was conducted by using BRUKER VERTX 70 in a range of 12500-350 cm^{-1}. Nuclear magnetic resonance (NMR) measurement was obtained by using Varian Unity INOVA 400NB with the solvent of deuterated chloroform ($CDCl_3$).

Results and discussion

In a typical experiment, the Gemini surfactant is first dissolved in water, making a light yellowish color (Figure S1a in SI). With the addition of $AgNO_3$ and $HAuCl_4$, the yellowish solution becomes brownish because of the formation of $AuBr_4^-$ complex (Figure S1b).[48] In the presence of unsaturated C=C bond, Au^{3+} can be gradually reduced to Au^+ (as illustrated in Figure 1a), as evidenced by the color change from brownish to yellowish (Figure S1c). Upon the addition of ascorbic acid and gold seed, the yellowish solution gradually becomes reddish, bluish, and eventually dark reddish within several hours, indicating the formation of gold nanoparticles. Figure 1b shows a digital image of the as-obtained product. It is clear that the color of the product is uniform everywhere in the flask, suggesting the great uniformity of nanoparticles. The UV-vis spectrum (Figure 1d) shows that the obtained product has a sharp peak around 950 nm, implying high morphological yield of the product, which has been further confirmed by the TEM measurement. As shown in Figure 1c, monodispersed AuNRs with length around 106 nm and diameter around 17 nm have been successfully prepared. From both TEM and UV-vis characterization, we can claim that the morphological yield of AuNRs is over 95%, which is good enough for most of the applications.

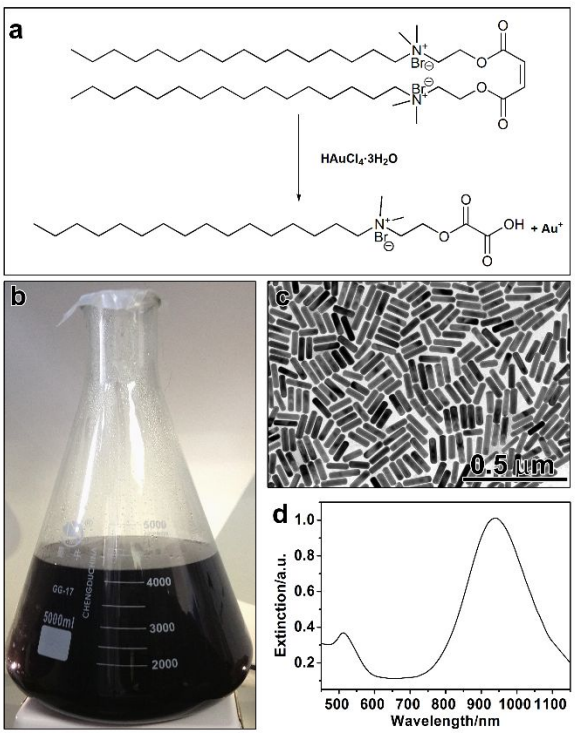

Figure 1. (a) Schematic illustration of the pre-reduction of Au^{3+} by P16-8-16. (b) Digital image of the as-prepared AuNRs with the total volume over 4,000 mL, (c) TEM image and (d) UV-vis spectrum of the as-prepared AuNRs. [$HAuCl_4$] = 0.25 mM, [P16-8-16] = 12 mM, [$AgNO_3$] = 0.4 mM, [ascorbic acid] = 0.32 mM, [HCl] = 10 mM, and the volume of seed solution is 20 mL.

Recently, it is reported that the pre-reduction of Au^{3+} into Au^+ may be beneficial to the synthesis of anisotropic gold nanostructures.[29, 30, 49] For example, Ye and Murray demonstrated that some additives, such as aromatic additives or unsaturated fatty acids, can be used as a secondary reagent in CTAB/CTAC system to improve the synthesis.[7, 29, 30] Liz Marzán *et al* also pointed out that the pre-reduction of Au^{3+} into Au^+ plays an important role in such systems.[43] The pre-reduction process may kinetically control the growth of AuNRs and the negative charged additives can help to improve the monodispersity and size uniformity of AuNRs. As illustrated in Figure 1a, it is believed that the presence of unsaturated C=C bond in P16-8-16 can play the same role as that of aromatic additives or unsaturated fatty acids. To confirm this assumption, Fourier transform infrared spectroscopy (FTIR) and nuclear magnetic resonance (NMR) measurements have been performed. As shown in Figure 2a (red line), fresh P16-8-16 has three characteristic peaks around 1560 cm^{-1}, 1715cm^{-1} and 3010 cm^{-1}, which can be attributed to the vibration of C=C bond, C=O bond and C-H bond linked to the C=C bond in P16-8-16, respectively.[50] The absorption bands observed at 2922 cm^{-1} and 2852 cm^{-1} are ν_{asym}(C-H) and ν_{sym}(C-H), and the vibrationsat 1545 cm^{-1} and 1403 cm^{-1} are ν_{asym} (COO-) and ν_{asym}(COO-), respectively (Figure 2a).[51, 52] After reacting with excess Au^{3+} (the molar ratio between Au^{3+} and P16-8-16 is 5:1), two characteristic peaks around 1560 cm^{-1} and 3010 cm^{-1} disappear (black line in Figure 2a), indicating that the C=C bond has been oxidized by Au^{3+}. The oxidation process has been further confirmed by the NMR measurement, as plotted in Figure 2b. A peak with a chemical shift of 9.2 ppm is observed in the fresh P16-8-16, corresponding to the protons that connected to the C=C bond.[53] The low-field NMR peak can be attributed to the effects of ester group and long chain. After reaction, the peak at 9.2 ppm disappears and a new peak at around 11.3 ppm is observed. This new peak can be assigned to the protons in the carboxyl group, indicating that the C=C bond has been oxidized into carboxyl groups by Au^{3+}.[53] Peaks in the range of 0.5-4 ppm can be assigned to the protons in the alkyl chain.[54]

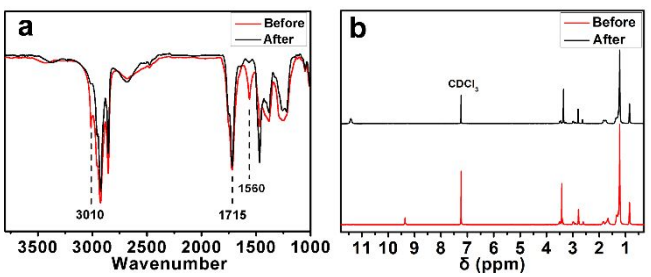

Figure 2. (a) FTIR spectra of the Gemini surfactant: before (red line) and after (black line) reacting with Au^{3+}, (b) NMR spectra of the Gemini surfactant: before (red line) and after (black line) reacting with Au^{3+}. $CDCl_3$ is used as the solvent.

The dimensions as well as the aspect ratio of AuNRs can be easily tailored by tuning the reaction parameters, such as the amount of gold seed, pH value, and the concentration of ascorbic acid. In the following experiments, the concentrations of P16-8-16 and $HAuCl_4$ are fixed at 12 mM and 0.25 mM, respectively. The total volumes of growth solution in the following experiments are fixed at 20 mL to cut the cost. It is found that less seed gives higher aspect ratio. As

show in Figure 3a, when the amount of gold seed is decreased from 0.16 mL to 0.1 mL and the other parameters are kept the same, the dimension of AuNRs changed from 61.0 ± 4.7 nm in length and 25.4 ± 3.5 nm in diameter to 74.7 ± 4.4 nm in length and 23.4 ± 3.4 nm in diameter, giving an aspect ratio of 3.2. Lower pH value leads to higher aspect ratio. As shown in Figure 3b, when the concentration of HCl is 6mM, the as-obtained product has an average length of 90.7 ± 4.1 nm and diameter of 18.9 ± 4.2 nm, giving an aspect ratio of 4.8 (Figure 3b). As the concentration of HCl increased to 10 mM, the length of products is about 97.5 ± 4.8 nm, while the diameter is around 17.7 ± 4.0 nm, giving an aspect ratio of 5.5 (Figure 3c). On the other hand, less ascorbic acid gives rise to higher aspect ratio. When the concentration of ascorbic acid is decreased from 0.64 mM to 0.32 mM, the dimension of AuNRs is 105.2 ± 11.9 nm in length and 16.7 ± 4.0 nm in diameter, giving an aspect ratio of 6.3, as evidenced by the TEM measurement in Figure 3d.

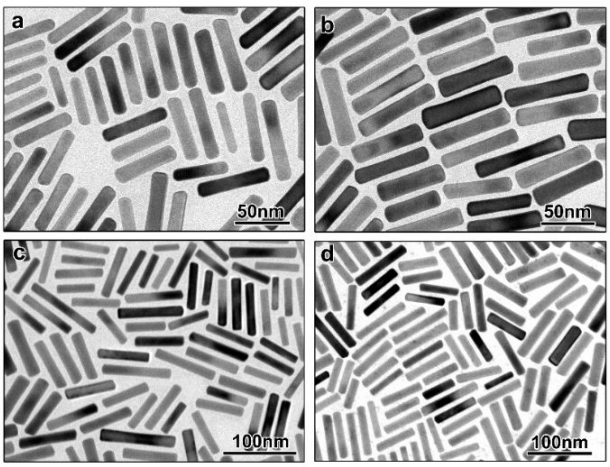

Figure 3. (a-d) TEM images of the obtained AuNRs with different dimensions: (a) l = 74.7 ± 4.4 nm, d = 23.4 ± 3.4 nm; (b) l = 90.7 ± 4.8 nm, d = 18.9 ± 3.5 nm; (c) l = 97.5 ± 4.8 nm, d =17.7 ± 4.0 nm; (d) l = 105.2 ± 11.9 nm, d = 16.7 ± 4.0 nm. Reaction conditions are listed in Table S1.

Because the SPR property is determined by the aspect ratio of AuNRs, the SPR peak can therefore be easily tuned by simply varying the reaction parameters. As shown in Figure 4a, by altering the volume of seed solution, silver concentration, pH value as well as the concentration of ascorbic acid, the longitudinal SPR wavelengths can be tuned from about 660 nm to 960 nm. AuNRs with aspect ratio of 2.4 and SPR peak around 660 nm can be obtained when the volume of seed solution is 0.16 mL. As the aspect ratio increased to 3.2, the SPR peak red-shifts to 720 nm in the presence of 0.1 mL of seed solution (Figure 4b). On the other hand, lower pH value and less ascorbic acid gives rise to higher aspect ratio and longer SPR wavelength. As shown in Figure 4, when the concentration of ascorbic acid is 0.64 mM, the obtained AuNRs have an aspect ratio of about 4.1, giving a SPR wavelength of 760 nm. When the concentration of ascorbic acid is decreased to 0.32 mM, the aspect ratio and SPR wavelength increase to about 6.3 and 960 nm, respectively. Hereby, the present work has provided a reliable protocol for synthesis of AuNRs with high morphological yield and tunable SPR property.

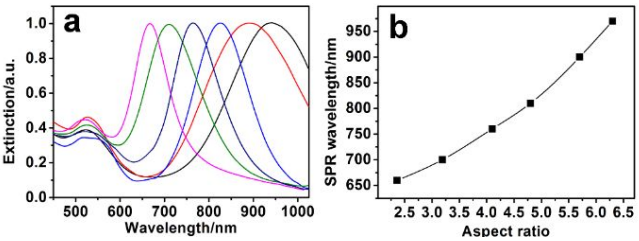

Figure 4. UV-vis spectra (a) and the plot of SPR peak position as a function of aspect ratio (b) of AuNRs obtained under different reaction conditions. Reaction conditions are listed in Table S1.

The detailed synthesis process has been investigated systematically. We first examined the role of silver ions. It is well known that silver ion is critical to the seeded growth of AuNRs, although the function of silver ions is still under debate.[14] Without silver ions, only spherical gold nanoparticles are observed (as shown in Figure S2). In the presence of silver ions, a significant improvement in the morphological yield is obtained, which is in well agreements with the previous reports on the effects of silver. As shown in Figure 5, when the concentration of silver ions is 0.15 mM, the morphological yield of AuNRs is about 90 % (Figure 5a). When the concentration of silver ions is further increased to 0.25 mM, an improvement in the morphological yield can be achieved (> 95 %), indicating that silver is critical for the synthesis of AuNRs with high morphological yield. No obvious improvement in the morphological yield can be observed when the concentration of silver ions is further increased to 0.4 mM and 0.5 mM. In addition, the dimensions of the AuNRs can be tuned by varying the concentration of silver ions. For example, as shown in Figure 5e, when the concentration of silver ions is 0.15 mM, the aspect ratio is about 3.2, giving a longitudinal SPR wavelength of~ 720 nm (black line). The aspect ratio increases to ~ 4.7 when the concentration of silver ions is increased to 0.25 mM. Correspondingly, the longitudinal SPR peak shifts to about 810 nm (red line in Figure 5e). Further increasing the concentration of silver ions to 0.4 mM and 0.5 mM shifts the longitudinal SPR wavelength to 880 nm (blue line in Figure 5e, aspect ratio = 5.6) and 960 nm (magenta line in Figure 5e, aspect ratio = 6.3), respectively. As plotted in Figure 5f, higher concentration of silver ions leads to higher aspect ratio of AuNRs, which is consistent with previous reports. It is worth pointing out that the characteristic peak of spherical Au nanoparticles at 520 nm is weak in all the UV-vis spectra, implying the high morphological yield of the obtained AuNRs, which is in great agreement with TEM characterizations (Figure 5a-d). Further increasing the concentration of silver ions to 1 mM will significantly slow down the reaction process.

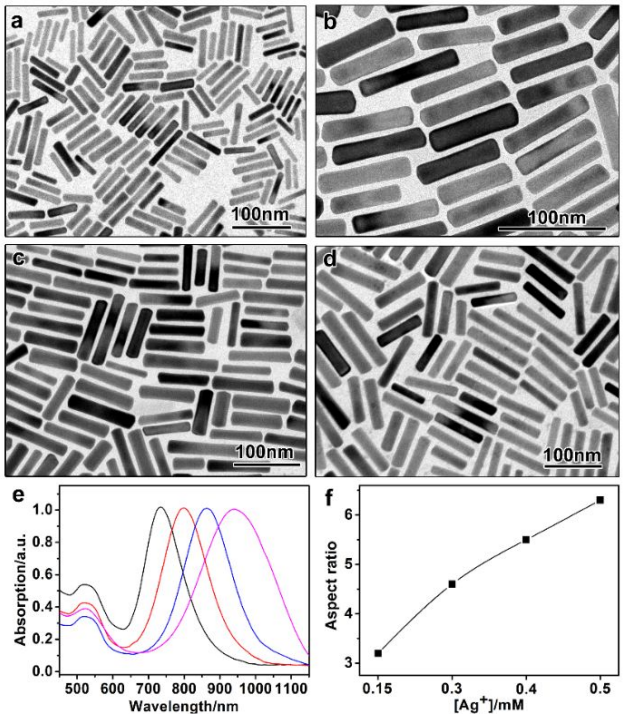

Figure 5. TEM images (a-d), UV-vis spectra (e) and plot of aspect ratio as a function of silver ions concentration (f) of AuNRs obtained in the presence of different concentration of silver ions. Reaction conditions: (a and black line in e) $[Ag^+]$ = 0.15 mM, (b and red line in e) $[Ag^+]$ = 0.25 mM, (c and blue line in e) $[Ag^+]$ = 0.4 mM, (d and magenta line in e) $[Ag^+]$ = 0.5 mM. In all the reactions, [P16-8-16] = 12 mM, $[HAuCl_4]$ = 0.25 mM, [ascorbic acid] = 0.32 mM, [HCl] = 10 mM, and the volume of seed solution is 0.1 mL.

As the Gemini surfactant appears to be the most critical reagent in this process, its role has been investigated carefully. In the absence of P16-8-16, only spherical particles can be obtained, as indicated by a broad peak around 520 nm observed in the UV-vis spectrum (Figure S3a). TEM characterization also confirms that only large spherical Au nanoparticles with size around 80 nm can be obtained (Figure S3b). As shown in Figure 6, when the concentration of P16-8-16 is 12 mM, monodispersed AuNRs with an estimated length of 104.7 ± 11.6 nm and diameter of 16.5 ± 4.0 nm are obtained, indicating that G16-8-16 can stabilize AuNRs at a very low concentration (Figure 6a). In the presence of higher concentration of P16-8-16, AuNRs become fatter with an average length of 86.9 ± 15.1 nm and diameter of 22.4 ± 7.2 nm, as shown in Figure 6b. Another noticeable change in the morphology is that the end part becomes wider than the middle part, giving a shape of "dumbbell". When the concentration of P16-8-16 is further increased to 21 mM (Figure 6c) and 24 mM (Figure 6d), the morphological change becomes more noticeable. As shown in Figure 6d, "dog-bone" like nanostructures can be observed with the diameter in the end part and the middle part is 50.3 ± 15.4 nm and 20.1 ± 10.3 nm, respectively. Moreover, some of the nanoparticles even further evolve to quadruped-like structure when the concentration of P16-8-16 is 24 mM (Figure 6d). It is worth pointing out that the shape evolution induced by the different concentration of P16-8-16 can cause some differences in the SPR property. As shown in Figure 6e, the longitudinal SPR peak blue shifts to shorter wavelengths as the concentration of P16-8-16 increased from 18 mM to 24 mM, indicating the decrease in aspect ratios (Figure 6f), which is in great agreement with the TEM characterization. Additionally, the overall shape of the extinction spectra are somehow different as the shape evolving from nanorods to "dog-bones". As shown in Figure 6e, when the concentration of P16-8-16 is increased from 12 mM to 18 mM, a flat peak in the range of 500-600 nm is observed (blue line), which becomes more obvious when the concentration of P16-8-16 is further increased to 21 mM (black line) and 24 mM (red line), respectively. The flat peak may be attributed to the morphology change from "straight nanorods" to "curved dog-bones".

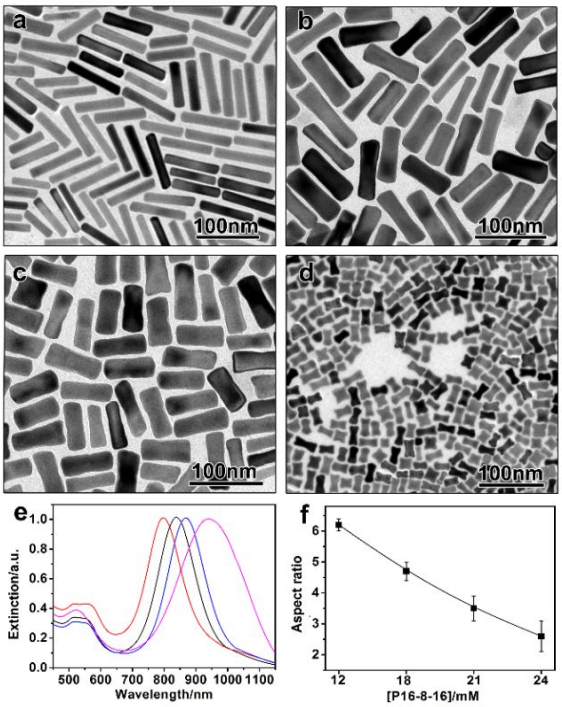

Figure 6. TEM (a-d) images, UV-vis spectra (e) and plot of aspect ratio as a function of P16-8-16 concentration (f) of AuNRs obtained in the presence of different concentration of P16-8-16. Reaction conditions: (a and magenta line in e) [P16-8-16] = 12 mM, (b and blue line in e) [P16-8-16] = 18 mM, (c and black line in e) [P16-8-16] = 21 mM, (d and red line in e) [P16-8-16] = 24 mM. In all the reactions, $[Ag^+]$ = 0.3 mM, $[HAuCl_4]$ = 0.25 mM, [ascorbic acid] = 0.32 mM, [HCl] = 10 mM, and the volume of seed solution is 0.04 mL.

To clearly reveal the role of Gemini surfactant in the shape evolution process, a systematic study has been carried out. High resolution transmission electron microscopy and selected area electron diffraction (SAED) are used to reveal the crystal structure of the obtained gold nanoparticles. As shown in Figure 7, results from HRTEM images and SAED patterns clearly show that the obtained gold nanoparticles (from nanorods to "dog bones") are single-

crystals with a face-centered cubic (*fcc*) structure. Although the shapes are quite different, the surface facets are the same, as evidenced by the measured lattice distance of 0.205 nm corresponding to Au (200) spacing, indicating that the growth directions of the different gold structures are the same. The shape evolution from nanorods to dumbbells" and "dog bones" may be ascribed to an overgrowth process at the end of nanorods.

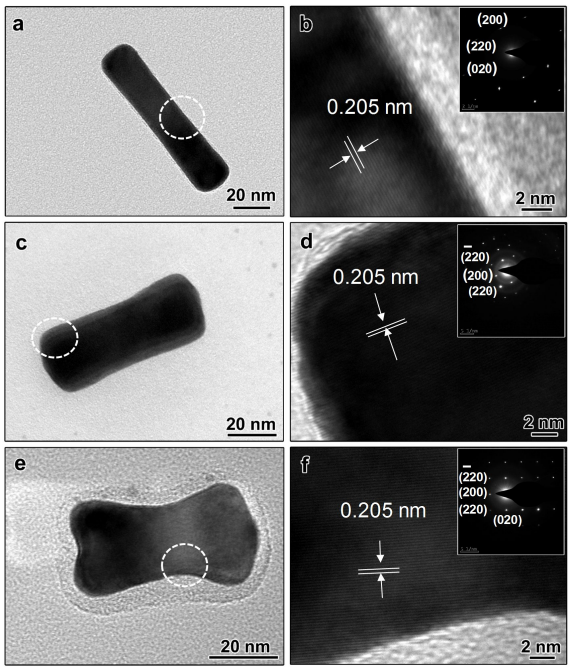

Figure 7. HRTEM images and SAED patterns of AuNRs obtained in the presence of different concentration of P16-8-16: (a, b) 12mM, (c, d) 18 mM, (e, f) 24 mM. In all the reactions: [Ag^+] = 0.3 mM, [$HAuCl_4$] = 0.25 mM, [ascorbic acid] = 0.32 mM, [HCl] = 10 mM, and the volume of seed solution is 0.04 mL.

The above results indicate that P16-8-16 has played a critical role in the shape evolution process. At the same time, we noticed that the reaction becomes much slower in the presence of higher concentration of P16-8-16. The reaction can be completed within 8 hours in the presence of 12 mM P16-8-16. However, it takes almost 24 hours when the concentration of P16-8-16 is increased to 24 mM. When the concentration of bromide ions is further increased to 0.1 M, only a few irregular nanoparticles can be observed after 7 days (data not shown here). It is well known that bromide ions can slow down the reaction by coordinating with gold ions to form more stable $AuBr_4^-$ and $AuBr_2^-$.[55] Besides, the shape evolution process observed in our system is similar to previous reports in which the overgrowth of AuNRs leads to a fatter or curved AuNRs.[46, 56] We therefore suspect that bromide ions might be the most important factor in determining the shape evolution process.

To confirm this assumption, the effect of bromide ions has been carefully investigated. In a typical process, additional bromide ions are introduced into the growth solution by using potassium bromide (KBr) as the bromide source. When the concentration of P16-8-16 is 12 mM, the total concentration of bromide ions is 24 mM. Under this condition, straight AuNRs are obtained (Figure 8a). A sharp peak at about 950 nm is observed in UV-vis spectrum, corresponding to the longitudinal SPR wavelength of AuNRs (blue line in Figure 8d). In the following experiments, the concentration of P16-8-16 is fixed at 12 mM. With the addition of 12 mM KBr solution, the total concentration of bromide ions increases to 36 mM, which is the same as that of pure 18 mM P16-8-16. Curved nanorods with wider end part are obtained. The average length is 82.3 ± 10.3 nm, the diameter in the middle part and end part are 22.9 ± 9.1 nm and 30 ± 3.2 nm (Figure 8b), respectively, which is very similar to the product obtained in the presence of 18 mM P16-8-16 (l = 86.9 ± 15.1 nm, d = 22.4 ± 7.2 nm in the middle part and d = 28.8 ± 3.8 nm in the end part). This result suggests that the shape change may be caused by the higher concentration of bromide ions. When the KBr concentration is further increased to 24 mM ([Br^-] is 48 mM in total), "dog-bones" are obtained with an average length of 46.9 ± 14.6 nm and diameter of 22.4 ± 10.8 nm in middle part (31.4 ± 9.3 nm in the end part) (Figure 8c), which is similar to the obtained product in the presence of 24 mM of P16-8-16 (l = 50.3 ± 15.4 nm, d = 20.1 ± 10.3 nm in the middle part and d = 35.1 ± 12.1 nm). In addition to the similar structure, the SPR property shows similar trend. As shown in Figure 8d, a flat peak can be observed in the UV-vis spectra when additional KBr is introduced into the reaction system, further confirming that the shape evolution can be attributed to the increased concentration of bromide ions. It is worth pointing out that when the concentration of bromide ions is further increased to 0.1 M, the duration of the growth process is greatly extended. Only a few spherical gold nanoparticles are obtained after 7 days (data not shown here).

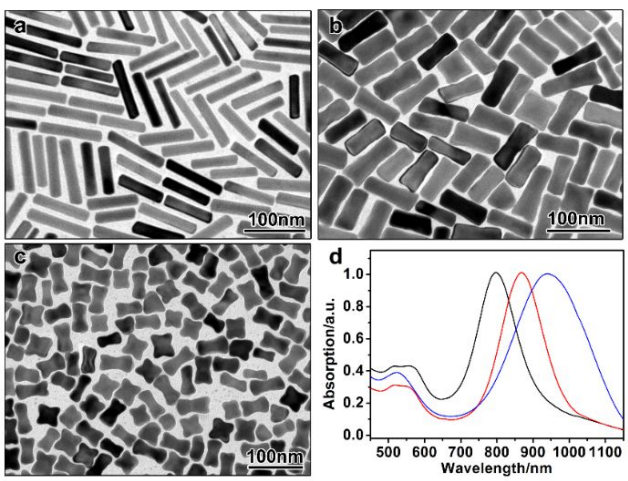

Figure 8. TEM images (a-c) and UV-vis spectra (d) of AuNRs obtained with different concentration of bromide ions. Reaction conditions: (a and blue line in d) [P16-8-16] = 12 mM, [KBr] = 0 mM; (b and red line in d) [P16-8-16] = 12 mM, [KBr] = 12 mM; (c and black line in d) [P16-8-16] = 12mM, [KBr] = 24 mM. In all the reactions: [Ag^+] = 0. 3 mM, [$HAuCl_4$] = 0.25 mM, [ascorbic acid] = 0.32 mM, [HCl] = 10 mM, and the volume of seed solution is 0.04 mL.

Based on the above results, a plausible mechanism has been proposed. With the increased concentration of P16-8-16, the concentration of bromide ions is increased, which can significantly inhibit the reaction kinetics.[55] For AuNRs, the aspect ratio is determined by the growth rate of the rod length and rod diameter. Generally, the growth rate of the rod length is much faster than the rod diameter in the early stage of growth, leading to the formation of AuNRs with high aspect ratio.[26, 57] With the increased concentration of bromide ions, the fast growth rate of rod length is greatly reduced in the early stage because of the complex effect between gold ions and bromide ions, resulting in AuNRs with lower aspect ratio. In the later stage of growth, most of the Au^+ ions are reduced to form AuNRs. During this grow process, the growth rate is further decreased because of the consumption of gold ions and ascorbic acid, resulting in a non-uniform growth of AuNRs.[26] It is generally accepted the density of capping ligands at the corners of AuNRs is lower than that at the sides,[14] leading to a much poorer "blocking" effect at corners than that at the sides. Hence, we can conclude that the shape evolutions of AuNRs are induced by the inverse kinetic effect of bromide ions, resulting in the non-uniform growth of AuNRs at the ends to form "dog bones".

Conclusions

In summary, a reliable protocol has been developed to synthesize AuNRs with high morphological yield and tailored shapes in a large-scale and cost-effective way. By using an industrial grade Gemini surfactant (P16-8-16) as the surfactant, the cost of surfactant is only about 0.7 % of the total cost. Compared to traditional protocols, this method can cut the cost by up to 90%. Monodispersed AuNRs can be obtained even when the total volume of reaction is over 4L, making it promising for practical applications. It is believed that P16-8-16 can act as both capping ligand and weak reducing agent that can pre-reduce Au^{3+} to Au^+. The shape of AuNRs can be tuned from nanorods to "dog-bones" by simply altering the concentration of P16-8-16. Systematic studies reveal that bromide ions are critical to the shape evolution process by tuning the reaction kinetics. This research may not only help to promote the industrial application of nanomaterials but also shed some light on the design and synthesis of anisotropic nanostructures.

Acknowledgements

We thank the funding support from the National Natural Science Foundation of China (21401135) and the Natural Science Foundation of Jiangsu Province (BK20140304). Y.X. thanks the postdoctoral starting funding support from Soochow University.

Notes and references

Jiangsu Key Laboratory for Carbon-Based Functional Materials & Devices, Institute of Functional Nano and Soft Materials (FUNSOM) and Collaborative Innovation Center of Suzhou Nano Science and Technology, Soochow University, Suzhou 215123, P. R. China

* Corresponding author: qiaozhang@suda.edu.cn

§ Y. Xu and Y. Zhao contributed equally.

Electronic Supplementary Information (ESI) available: [Digital pictures during the growth process of AuNRs, TEM images of nanoparticles obtained without P16-8-16 or silver, HRTEM image and SAED patter of quadrupeds]. See DOI: 10.1039/b000000x/

1. S. Eustis and M. A. El-Sayed, *Chem. Soc. Rev.*, 2006, **35**,209-217.
2. M. Hu, J. Chen, Z.-Y. Li, L. Au, G. V. Hartland, X. Li, M. Marquez and Y. Xia, *Chem. Soc. Rev.*, 2006, **35**, 1084-1094.
3. Y. Yin and A. P. Alivisatos, *Nature*, 2005, **437**, 664-670.
4. H. P. Liang, H. M. Zhang, J. S. Hu, Y. G. Guo, L. J. Wan and C. L. Bai, *Angew. Chem. In. Ed.*, 2004, **43**, 1540-1543.
5. S. Pedireddy, H. K. Lee, W. W. Tjiu, I. Y. Phang, H. R. Tan, S. Q. Chua, C. Troadec and X. Y. Ling, *Nat. Commun.*, 2014, **5**,4947.
6. C. B. Gao, J. Vuong, Q. Zhang, Y. D. Liu and Y. D. Yin, *Nanoscale*, 2012, **4**, 2875-2878.
7. X. C. Ye, L. H. Jin, H. Caglayan, J. Chen, G. Z. Xing, C. Zheng, V. Doan-Nguyen, Y. J. Kang, N. Engheta, C. R. Kagan and C. B. Murray, *ACS Nano*, 2012, **6**, 2804-2817.
8. J. Wang, C.-K. Tsung, R. C. Hayward, Y. Wu and G. D. Stucky, *Angew. Chem. In. Ed.*, 2004, **44**, 332-336.
9. Z. Y. Tang, N. A. Kotov and M. Giersig, *Science*, 2002, **297**, 237-240.
10. J. Lai, L. Zhang, W. Niu, W. Qi, J. Zhao, Z. Liu, W. Zhang and G. Xu, *Nanotechnology*, 2014, **25**, 12560.
11. Q. Zhang, N. Li, J. Goebl, Z. Lu and Y. Yin, *J. Am.Chem. Soc.*, 2011, **133**, 18931-18939.
12. L. Chen, F. Ji, Y. Xu, L. He, Y. Mi, F. Bao, B. Sun, X. Zhang and Q. Zhang, *Nano Lett.*, 2014,**14**, 7201-7206.
13. X. Chen, J. J. Zhang, J. Xuan and J. J. Zhu, *Nano Res.*, 2009, **2**, 210-219.
14. S. E. Lohse and C. J. Murphy, *Chem. Mater.*, 2013, **25**, 1250-1261.
15. X. H. Huang, S. Neretina and M. A. El-Sayed, *Adv. Mater.*, 2009, **21**, 4880-4910.
16. X. H. Huang, I. H. El-Sayed, W. Qian and M. A. El-Sayed, *J. Am.Chem. Soc.*, 2006, **128**, 2115-2120.
17. X. H. Huang, I. H. El-Sayed, W. Qian and M. A. El-Sayed, *Nano Lett.*, 2007, **7**, 1591-1597.
18. J. V. Jokerst, A. J. Cole, D. Van de Sompel and S. S. Gambhir, *ACS Nano*, 2012, **6**, 10366-10377.
19. E. C. Dreaden, A. M. Alkilany, X. Huang, C. J. Murphy and M. A. El-Sayed, *Chem. Soc. Rev.*, 2012, **41**, 2740-2779.
20. R. Huschka, J. Zuloaga, M. W. Knight, L. V. Brown, P. Nordlander and N. J. Halas, *J. Am.Chem. Soc.*, 2011, **133**, 12247-12255.
21. L. B. Wang, Y. Y. Zhu, L. G. Xu, W. Chen, H. Kuang, L. Q. Liu, A. Agarwal, C. L. Xu and N. A. Kotov, *Angew. Chem. In. Ed.*, 2010, **49**, 5472-5475.
22. L. Vigderman, B. P. Khanal and E. R. Zubarev, *Adv. Mater.*, 2012, **24**, 4811-4841.
23. Y. Jiang, F. Meng, D. Qi, P. Cai, Z. Yin, F. Shao, H. Zhang, F. Boey and X. Chen, *Small*, 2013, **9**, 2260-2265.
24. R. A. Alvarez-Puebla, A. Agarwal, P. Manna, B. P. Khanal, P. Aldeanueva-Potel, E. Carbo-Argibay, N. Pazos-Perez, L. Vigderman, E. R. Zubarev, N. A. Kotov and L. M. Liz-Marzan, *Proc. Natl. Acad. Sci. USA*, 2011, **108**, 8157-8161.
25. A. F. Stewart, A. Lee, A. Ahmed, S. Ip, E. Kumacheva and G. C. Walker, *ACS Nano*, 2014, **8**, 5462-5467.
26. K. Park, L. F. Drummy, R. C. Wadams, H. Koerner, D. Nepal, L. Fabris and R. A. Vaia, *Chem. Mater.*, 2013, **25**, 555-563.

27. J. Perez-Juste, L. M. Liz-Marzan, S. Carnie, D. Y. C. Chan and P. Mulvaney, *Adv. Funct. Mater.*, 2004, **14**, 571-579.
28. J. Perez-Juste, I. Pastoriza-Santos, L. M. Liz-Marzan and P. Mulvaney, *Coordin. Chem. Rev.*, 2005, **249**, 1870-1901.
29. X. Ye, Y. Gao, J. Chen, D. C. Reifsnyder, C. Zheng and C. B. Murray, *Nano Lett.*, 2013, **13**, 2163-2171.
30. X. Ye, C. Zheng, J. Chen, Y. Gao and C. B. Murray, *Nano Lett.*, 2013, **13**, 765-771.
31. B. Goris, S. Bals, W. Van den Broek, E. Carbo-Argibay, S. Gomez-Grana, L. M. Liz-Marzan and G. Van Tendeloo, *Nat. Mater.*, 2012, **11**, 930-935.
32. M. Grzelczak, A. Sanchez-Iglesias, B. Rodriguez-Gonzalez, R. Alvarez-Puebla, J. Perez-Juste and L. M. Liz-Marzan, *Adv. Funct. Mater.*, 2008, **18**, 3780-3786.
33. T. H. Ha, H.-J. Koo and B. H. Chung, *J. Phys. Chem. C*, 2007, **111**, 1123-1130.
34. J. Wang, Y. F. Li and C. Z. Huang, *J. Phys. Chem. C*, 2008, **112**, 11691-11695.
35. N. Almora-Barrios, G. Novell-Leruth, P. Whiting, L. M. Liz-Marzan and N. Lopez, *Nano Lett.*, 2014, **14**, 871-875.
36. J. E. Millstone, W. Wei, M. R. Jones, H. Yoo and C. A. Mirkin, *Nano Lett.*, 2008, **8**, 2526-2529.
37. B. Nikoobakht and M. A. El-Sayed, *Chem. Mater.*, 2003, **15**, 1957-1962.
38. S. K. Hait and S. P. Moulik, *Curr. Sci.*, 2002, **82**, 1101-1111.
39. D. Li, W. Fang, H. Wang, C. Gao, R. Zhang and K. Cai, *Ind. Eng. Chem. Res.*, 2013, **52**, 8109-8113.
40. K. Esumi, J. Hara, N. Aihara, K. Usui and K. Torigoe, *J. Colloid Interf. Sci.*, 1998, **208**, 578-581.
41. W. T. Wang, Y. C. Han, M. Y. Gao and Y. L. Wang, *Crystengcomm*, 2013, **15**, 2648-2656.
42. A. Guerrero-Martinez, J. Perez-Juste, E. Carbo-Argibay, G. Tardajos and L. M. Liz-Marzan, *Angew. Chem. In. Ed.*, 2009, **48**, 9484-9488.
43. L. Scarabelli, M. Grzelczak and L. M. Liz-Marzan, *Chem. Mater.*, 2013, **25**, 4232-4238.
44. X. Xu and M. B. Cortie, *Adv. Funct. Mater.*, 2006, **16**, 2170-2176.
45. L. F. Gou and C. J. Murphy, *Chem. Mater.*, 2005, **17**, 3668-3672.
46. F. Ratto, P. Matteini, F. Rossi and R. Pini,*J. Nanopart. Res.*, 2010, **12**, 2029-2036.
47. S. R. Jackson, J. R. McBride, S. J. Rosenthal and D. W. Wright, *J. Am.Chem. Soc.*, 2014, **136**, 5261-5263.
48. A. Usher, D. C. McPhail and J. Brugger, *Geochim. Cosmochim. Ac.*, 2009, **73**, 3359-3380.
49. Y. Xu, X. Wang, L. Chen, Y. Zhao, L. He, P. Yang, H. Wu, F. Bao and Q. Zhang, *J. Mater. Chem. C.*,2015,**3**, 1447-1451.
50. J. Tarasiewicz, R. Jakubas, I. Majerz, J. Baran, A. Gągor and A. Miniewicz, *Vib. Spectrosc.*, 2013, **66**, 93-103.
51. L. Van Hai, T. Chi Nhan Ha and T. Huy Ha, *Nanoscale Res. Lett.*, 2013, **8**, 1-10.
52. J. Tang, K. W. Kemp, S. Hoogland, K. S. Jeong, H. Liu, L. Levina, M. Furukawa, X. Wang, R. Debnath, D. Cha, K. W. Chou, A. Fischer, A. Amassian, J. B. Asbury and E. H. Sargent, *Nat. Mater.*, 2011, **10**, 765-771.
53. H. K. Can, Z. M. O. Rzaev and A. Güner, *J. Mol. Liq.*, 2004, **111**, 77-84.
54. F. Hubert, F. Testard and O. Spalla, *Langmuir*, 2008, **24**, 9219-9222.
55. C. Bullen, P. Zijlstra, E. Bakker, M. Gu and C. Raston, *Cryst. Growth Des.*, 2011, **11**, 3375-3380.
56. B. N. Khlebtsov, V. A. Khanadeev, J. Ye, G. B. Sukhorukov and N. G. Khlebtsov, *Langmuir*, 2014, **30**, 1696-1703.
57. J. A. Edgar, A. M. McDonagh and M. B. Cortie, *ACS Nano*, 2012, **6**, 1116-1125.

